Calculations of giant magnetoresistance in Fe/Cr trilayers using layer potentials determined from *ab-initio* methods

M. Pereiro[1,2]‡ , D. Baldomir[1,2], S. V. Man'kovsky[3], K. Warda[4], J. E. Arias[2], L. Wojtczak[4], and J. Botana[1,2]

[1]Departamento de Física Aplicada, Universidade de Santiago de Compostela, Santiago de Compostela E-15782, Spain.
[2]Instituto de Investigacións Tecnolóxicas, Universidade de Santiago de Compostela, Santiago de Compostela E-15782, Spain.
[3]Institute for Metal Physics of the National Academy of Sciences of Ukraine, Kiev, Ukraine.
[4]Solid State Physics Department, University of Łódź, ul. Pomorska 149/153, 90-236 Łódź, Poland

Abstract. The *ab initio* full-potential linearized augmented plane-wave method explicitly designed for the slab geometry was employed to elucidate the physical origin of the layer potentials for the trilayers nFe/3Cr/nFe(001), where n is the number of Fe monolayers. The thickness of the transition-metal ferromagnet has been ranged from $n = 1$ up to $n = 8$ while the spacer thickness was fixed to 3 monolayers. The calculated potentials were inserted in the Fuchs-Sondheimer formalism in order to calculate the giant magnetoresistance (GMR) ratio. The predicted GMR ratio was compared with the experiment and the oscillatory behavior of the GMR as a function of the ferromagnetic layer thickness was discussed in the context of the layer potentials. The reported results confirm that the interface monolayers play a dominant role in the intrinsic GMR.

PACS numbers: 71.15.Ap, 75.47.De, 75.70.Ak, 75.70.Cn

‡ Author to whom any correspondence should be addressed (fampl@usc.es).

1. Introduction

Advances in ultrathin-film fabrication techniques have made possible, only quite recently, the construction of thin magnetic transition metal layers, separated by very thin non-magnetic layers (spacers), forming superlattices or sandwiches. The multilayer system Fe/Cr/Fe has played a fundamental role because the giant magnetoresistance (GMR) was first discovered on it [1]. Control of the spacer thickness with great accuracy, keeping constant the width of the magnetic layers, has been the main preoccupation of experimentalists for a long time, because this factor is one of the basic conditions for obtaining great values of GMR as well as the coupling constant between the magnetic layers, but the variation of the magnetic layer thickness and its influence on GMR had remained without experimental measurements until quite recently [2, 3]. This fact is understandable because most of these experiments were guided by the so far existing models in either the quantum-well [4] (QW) or the Ruderman-Kittel-Kasuya-Yosida (RKKY) picture [5]. These models study the oscillatory exchange coupling of the magnetic layers, mediated by the electrons in the spacer, as a function of the spacer thickness and remaining the ferromagnetic layer thickness constant in most of the studied layered structures. However, in this work we focus our attention on the GMR effect produced by the variation of the magnetic layer thickness and surprisingly we have found an oscillating magnetic behavior of the magnetic layers. The explanation resides more in the presence of QW states than invoking the RKKY-like models, as we will see below.

Nowadays, it is well known that the interface between layers plays a dominant role in the GMR and obviously it depends strongly on the materials of the sample [6]. However, the controversy about whether GMR originates from bulk or interface scattering is still open [7]. This article will threw some light on this controversy because we calculate the contribution to GMR coming from the bulk and the interface layers. Moreover, we will show that the magnetic properties change as a function of the ferromagnetic layer thickness (FLT) and the contribution to the GMR effect of this system is not negligible as we will prove using the Boltzmann model where the potentials are calculated from the *ab initio* data. Thus, we obtain the density of states (DOS) and energy bands for different FLT and through them we can calculate the potentials. A remarkable fact is that the former potentials are numerically close to those reported by Hood and Falicov [8, 9] which were chosen without an explicit justification. Thanks to considering the full electronic structure of these materials, we are able to obtain directly the magnetoresistance of these Fe/Cr/Fe samples in a good agreement with the experiment, at least for a certain interval of the ferromagnetic layer thickness [3]. It should be stressed that our *ab initio* calculations and the interpretation through Boltzmann formalism can give us information about some confusion areas where the mesoscopic concepts play a fundamental role such as in the case of the interface. For systems of reduced dimensions (in this article corresponds to a number of iron monolayers (ML) less than four) the physical magnitudes such as the magnetic moments, conductivity or even the spin change

drastically their behavior, having striking consequences for the magnetoresistance effect like for example a considerable enhancement of the GMR ratio.

In the present article, we investigate the GMR for the layer potentials of Fe/Cr/Fe trilayers determined by means of density functional theory (DFT) calculations as a function of the thickness of the Fe layer. Our study is also restricted to the case of current in plane geometry (CIP). Although the study of GMR versus the spacer thickness is well described in literature, only a few articles are devoted to the case of a variable ferromagnetic layer. Nevertheless, we have found that the study of this case is more suitable for investigating the intrinsic origen of GMR. In order to show and explain our results we have organized the article as follows: in Sec. 2 we present the method of calculation. The Fe/Cr/Fe trilayer system is described and the physical origin of the layer potentials is determined according to the DFT calculations. Likewise, a brief description of the effective electron masses is presented in the next subsection. After that, the transport model is introduced in such a way which allows us to use the data based on DFT calculations, in particular, for the relaxation time and the effective mass. The method is developed in order to describe the electronic transport of the Fe/Cr/Fe trilayers in analogy to the evolution of the Co/Cu multilayer conductivity [10]. In Sec. 3 the results of our calculations are discussed and the predictions for GMR properties are reported. Sec. 4 includes some remarks and a brief summary of the article.

Thus, the aim of the present article is to describe GMR properties by means of the data obtained within DFT method and applied to the Fuchs-Sondheimer formalism extended for trilayers.

2. Method of calculation and Computational details

2.1. Self-consistent calculations

Ab initio electronic structure calculations were performed within the framework of density functional theory in the local spin density approximation (LSDA). The exchange-correlation potential was used in the form of Vosko, Wilk, and Nusair [11]. As it was reported in Ref. [12], the use of LSDA instead of the generalized gradient approximation (GGA) in Fe/Cr trilayers is adequate because GGA improves only the geometry optimization, while the energy calculations (in particular, Fermi energy) are more or less the same. Since we use a fixed geometry and the transport properties depend only on the Fermi energy, it is not necessary at all to use the GGA. The Kohn-Sham equations [13] were solved using the full-potential linearized augmented plane wave (FP-LAPW) method in slab geometry [14, 15]. This method is extremely advantageous for computing the electronic structure of magnetic multilayers, because it was designed to take into account the slab geometry and the interaction between the outermost monolayers of the trilayer system and vacuum. Thus, our method guarantees that all trilayer systems investigated in this work are two-dimensional translational invariants. To our best knowledge, this is the first attempt to account specifically for the slab geometry of

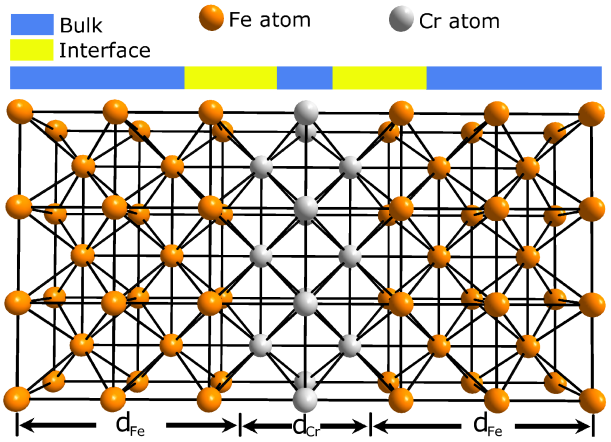

Figure 1. (Color online) Schematic picture of the generic $Fe_n/Cr_3(001)$ system. Blue and yellow color bar comprise the number of bulk and interface monolayers, respectively.

layers in contrast with other methodologies where the two-dimensional invariance is achieved by inserting vacuum layers to separate the interaction between the slabs [16]. The valence states were calculated in a scalar-relativistic approximation. A grid of 15 **k**-points in an irreducible wedge of the 2D BZ was used during self-consistent field (SCF) cycles and, once converged, a mesh of 45 **k**-points was considered to evaluate the final energy. Inside the muffin-tin spheres, basis functions with angular momentum components from 1 up to 8 were included. The charge density and potential within the muffin-tin spheres were expanded into the lattice harmonics with angular momentum from 1 up to 6. More than 60 Augmented Plane Waves per atom were used for the variational basis set.

2.2. Fe/Cr/Fe trilayers

Calculations were carried out for the slab consisting of 3 monolayers of Cr(001) and a variable number of Fe monolayers ($1 \leq n \leq 8$), where n is the number of Fe monolayers. The Fe layers are intrinsically ferromagnetic and the Cr layers are intrinsically antiferromagnetic (see column 4 of Tables 1 and 2). Figure 1 shows the schematic picture of 3 ML Cr in between 5 ML Fe for the bcc crystal orientation (001). We consider the monolayers to be in x-y plane and stacked along the z direction. It is well known that the magnetic properties, DOS, and energy bands depend strongly upon the atomic structures of the thin films. Therefore it is necessary to begin with an optimized structure for Fe_n/Cr_3 system. Nevertheless, no further attempt was made to relax the lattice parameter, i.e. the lattice constant for Fe and Cr was assumed to be Cr bcc bulk-like, that is, a_0=2.88 Å because we observed small differences in the obtained results when these constants were taken differently.

2.3. Layer potentials

The single band model representation leads to the energies

$$E_{\nu\sigma}(k) = \frac{1}{2} m^*_\sigma (v_\sigma(k))^2 + V_{\nu\sigma} \tag{1}$$

of electrons moving in the intrinsic potential $V_{\nu\sigma}$ with the spin σ in monolayer ν and velocity $v_\sigma(k)$. The intrinsic potentials require for these calculations to be determined on the basis of *ab initio* DFT calculations described in Sec. 2.1. Since these values are the electron energies corresponding to the bottom of conductivity band, they were taken to be equal to the energies of s, p-electrons in the Γ-point of 2D BZ, since we assume that these electrons have the main contribution to the conductivity. To describe the spin-dependent conductivity within our model, these energies were split by the value ΔE^{d-band} which is equal to the energy splitting of majority and minority-spin d-bands in Fe layers while in Cr layers the potential values were taken the same for both spin directions. Thus,

$$V_{\nu\sigma} = E^{s,p-band}_\nu(\mathbf{k}=0) - \zeta\sigma\Delta E^{d-band} \tag{2}$$

where $\zeta = 1$ for Fe slab and $\zeta = 0$ for Cr slab. Note that the spin electron in Bohr magneton units is $\sigma = +\frac{1}{2}$ for majority electrons and $\sigma = -\frac{1}{2}$ for minority electrons and the confinement of electrons within two-dimensional slab results in quantization of electron states in the direction perpendicular to the plane of this slab (z-direction). This quantum-size effect is essential, especially when the slab thickness is restricted to several atomic layers [17, 18, 19]. Therefore, we took it into account in our present calculations when the thickness of Fe film was equal to one-, two- or three atomic layers.

Since the quantum-well electronic states, in the case of ultrathin Fe films, are well localized in single atomic layer, we assume that the physical properties on this layer are determined mainly by the states which have the degree of localization in the layer more than 60%. The energy of the electron state in Γ-point corresponding to the energy band with high localization in the i-th atomic layer were taken as the i-th potential value. In the case of a thicker Fe film ($n \geq 4$) the electron states are more delocalized and they cannot be related to only one atomic layer, therefore we took in these cases the values of potentials $V_{\nu\sigma}$ common for a whole Fe film. The potential values in Cr film had always the same value for all Cr atomic layers. The variations of the layer potentials for $n \geq 4$ are expected to be quite small because of the delocalization of the electron states, such as is shown in Fig. 2.

2.4. Description of the effective mass

The effective mass parameter m^*_σ can be calculated by means of the standard procedure of DFT applied to the band structure calculations. An example of the complicated spin-dependent band structure provided by our DFT calculations is showed in Fig. 3 for the system Fe_5/Cr_3. The effective masses have been calculated as the second derivative of

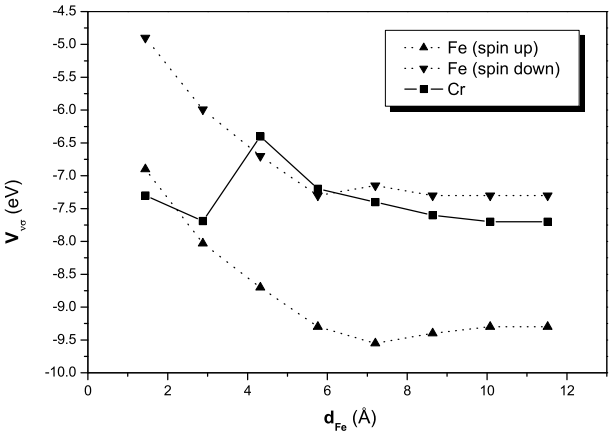

Figure 2. Dependence of the Fe majority (triangles), Fe minority (inverted triangles) and Cr (squares) layer potentials versus the FLT, d_{Fe}, for a fixed Cr thickness, $d_{Cr} = 4.32$ Å. For $n \leq 3$, the values of the layer potentials are given in average.

the s,p electronic band energy $E_\sigma(k)$ close to the Fermi level with respect to the Fermi wave vector k_F and evaluated on the Γ-point, according to the following relation

$$\frac{1}{m^*_\sigma} = \frac{1}{\hbar^2}\left(\frac{d^2E_\sigma(k)}{dk^2}\right)_{k=k_F}. \tag{3}$$

The energy band close to the Fermi level could always be approximated by a second-order polynomial in all considered systems. This argument is what underpins the parabolic approximation adopted in Sec. 2.3. The numerical evaluation of the effective masses is collected in Table 3. We can observe that our calculated effective masses are close to $4m_e$, that is the value assumed for the effective mass in Fe and Cr [8, 20]. To the best of our knowledge, no effective masses has been reported for Fe/Cr multilayers. In layered materials, we have only found the effective masses for Cu thin films deposited on the fcc Co film and they are in good agreement with the ones reported in table 3 [21].

2.5. The Transport Model

In order to consider the transport properties using the DFT data, the electronic transport for the Fe/Cr/Fe trilayers can be described by the Boltzmann formalism [8, 9, 22, 23, 24, 25] applied to the current in plane geometry. In every monolayer, the electric current is then determined by appropriate distribution functions in terms of the velocity v_z in the direction z perpendicular to the interface for the electron with spin up and spin down due to the translational symmetry in the plane of the film. The electrons involved in transport are embedded within the potentials $V_{\nu\sigma}$ of each monolayer ν. These potentials were determined using the DFT data in conjunction with Eq. (2).

With the aim of calculating the conductivity we write the Boltzmann equation in the relaxation time $\tau^*_{\nu\sigma}$ approximation for the distribution functions $g^\beta_{\nu\sigma}$ ($\beta = +, -$) which are determined with respect to the electric field applied in the direction of the electric current. The solutions are found taking into account the boundary conditions

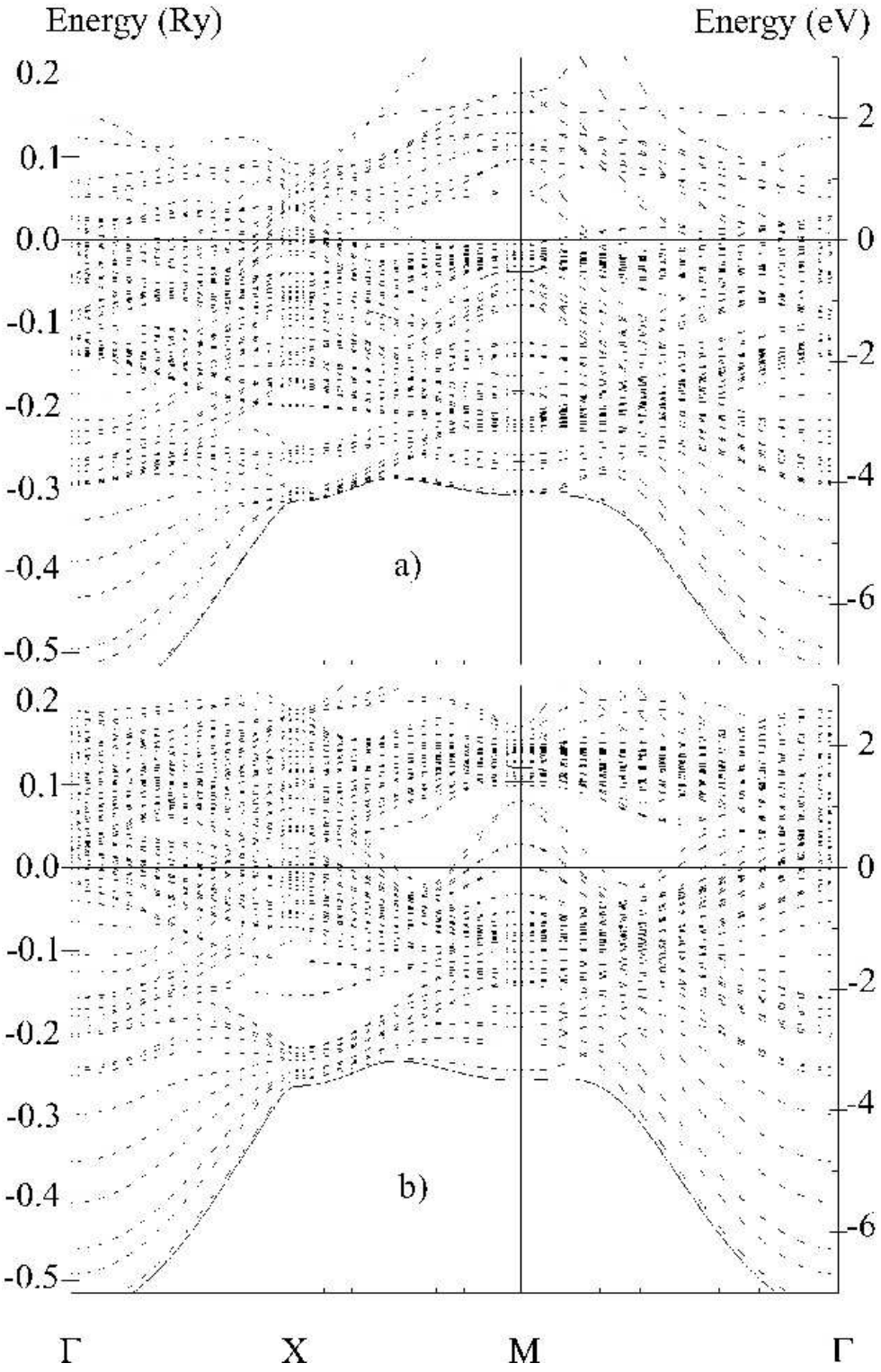

Figure 3. Energy bands of the majority-spin states (a) and the minority-spin states (b) for the system Fe_5/Cr_3. Solid lines represent the states with more than 50% of localization in the interface Fe layer. The Fermi level is at 0 eV.

at the outer surfaces, namely $g^{+}_{1\sigma} = P_{1\sigma} g^{-}_{1\sigma}$ (at z=0) and $g^{-}_{n\sigma} = P_{n\sigma} g^{+}_{n\sigma}$ (at z=$2(n+1)a_0$) with $g^{+}_{\nu\sigma}$ and $g^{-}_{\nu\sigma}$ standing for the solutions with $v^z \geq 0$ and $v^z < 0$, respectively. In order to extend our considerations to a more realistic case from the physical point of view, we define the specularity factor $P_{\nu\sigma}$ on the basis of the physical picture of the electrons involved in transport crossing through the potential barrier. In this case the value of $P_{\nu\sigma}$ corresponds to the specularity factor in the Fuchs-Sondheimer [26, 27] conductivity theory of thin films and leads to the effective result

$$P_{\nu\sigma}(\theta) = \frac{1 - \frac{(\chi_{\nu\sigma})^2 \cos^4\theta + 2}{1 + (\chi_{\nu\sigma})^2 \cos^4\theta}}{1 - \frac{(\chi_{\nu\sigma})^2 \cos^4\theta + 2}{(\chi_{\nu\sigma})^2 \cos^4\theta} \exp\left(-\frac{a_0}{\tau^*_{\nu\sigma} v^2 \cos\theta}\right)} \tag{4}$$

for ν ranging from 1 up to $2n+3$, that is an alternative version to other models which assume the coefficients for coherent transmission and specular reflections determined quantum mechanically by matching free electron wave functions and their derivatives at each interface (see Fig. 1). In Eq. (4), θ is the angle of incidence of electrons measured with respect to the z-axis. The parameter χ^{σ}_{F} is defined in terms of the Fermi velocity v_F as

$$\chi_{\nu\sigma} = \frac{2 m^*_{\sigma} \tau^*_{\nu\sigma} v_F^2}{\hbar} \tag{5}$$

where m^*_{σ} is the effective mass of σ electrons. From the physical point of view $\chi_{\nu\sigma}$ represents the ratio of the electron free path with respect to the de Broglie wavelength.

The distribution functions $g^{\alpha}_{\nu\sigma}$ depend on the relaxation times $\tau^*_{\nu\sigma}$ which can be evaluated in terms of the DFT calculations by means of the Fermi golden rule. The relaxation time can be expressed as follows [28]:

$$(\tau^*_{\nu\sigma})^{-1} = \frac{c}{\hbar} \rho_{\nu}(\varepsilon_F)(V_{\nu\sigma})^2 \tag{6}$$

where $\rho_{\nu}(\varepsilon_F)$ is the local density of states per monolayer ν at the Fermi energy, and c is the number of the scattering centers relative to the total number of atoms and it plays the role of a calibration factor in order to compare it with the average values in the case of samples discussed in literature. The Eq. (6) is important for thin films due to the presentation of the relaxation time distribution across a sample.

The total current in CIP geometry along the direction α defined by the electric field $\mathbf{E}^{\alpha}$ is obtained after averaging the current density over the whole thickness of the film and it is given by the relation [8, 9]

$$J^{\alpha} = \frac{-|e|}{d} \sum_{\nu=1,\sigma=\uparrow\downarrow}^{2n+3} \left[\frac{m^*_{\sigma}}{2\pi\hbar}\right]^3 \int_0^d \int v^{\alpha} g^{\beta}_{\nu\sigma}(\mathbf{v}, z, E^{\alpha}) d\mathbf{v} dz \tag{7}$$

where e is the electric charge and d is the length of the sample in the z direction. Assuming that the total conductivity of a sample can be defined as $\Sigma = 1/\rho = (dJ^{\alpha}/dE)_{E=0}$, and the magnetoresistance (MR) ratio as $\Delta\rho/\rho_s = (\rho_{\uparrow\downarrow} - \rho_{\uparrow\uparrow})/\rho_{\uparrow\downarrow}$, then the theoretical predictions of the GMR can be obtained straightforwardly. It is worth to emphasize that the MR ratio is found by calculating independently the resistivities for the parallel ($\rho_{\uparrow\uparrow}$) and the antiparallel ($\rho_{\uparrow\downarrow}$) alignment of the magnetic moments in

adjacent magnetic layers. The present approach remains in analogy to the calculations of Zahn *et al.* [10] who use the semiclassical Boltzmann theory with a spin independent relaxation time approximation. However, in our case, the relaxation time is not only a spin dependent but also shows a local character.

Concerning the problem of whether GMR originates from bulk or interface scattering, we consider the contribution to MR from bulk and interface layers separately. An example to allocate the bulk and interface layers where bulk and interface scattering occurs is plotted in Fig. 1. We have discretized the conductivity layer by layer with appropriate boundary conditions. Thus, the summation of the conductivity of the bulk layers and the conductivity of the interface layers was done independently to obtain the bulk and interface contributions to MR.

3. Results and discussion

3.1. Layer magnetic moments and potentials

First, we describe briefly the computational results obtained using the LAPW method. The numerical results of our calculations along with the layer potentials calculated according to Eq. (2) and the relaxation times provided by Eq. (6) are presented in Table 1 and Table 2.§

According to Fig. 4, the behavior of the magnetic moment versus the Fe film thickness for the interface Fe layer is non-monotonic in contrast with the surface Fe magnetic moment which ranges monotonically from 2.45 μ_B for $n = 1$ up to 2.98 μ_B for $n = 8$ (see fourth column of Table 1 and Table 2 for Fe(1) ML). We have also found the existence of highly localized states at Fe/Cr interface when the Fe film thickness is not too small ($n \geq 4$). These states can result in the onset of a big magnetic moment in the interface Fe layer as it takes place also at the surface. However, the localization of these states near the interface means that they should not be affected by the thickness of Fe film and the magnetic moments near Fe/Cr interface should be independent of Fe film thickness. This is a feature that in our opinion, is due to the QW states, which are delocalized throughout the slab and their energy changes together with increase of the Fe film thickness [29]. The QW states have a resonance with the interface states for $n = 4, 6, 8$. Consequently, the interface states become less localized which results in a decrease of their exchange splitting as well as in a decrease of the interface Fe magnetic moment. The opposite behavior is found for the case $n = 5, 7$ leading to an increase of the interface Fe magnetic moment, such as is shown in Fig. 4.

In this paragraph, our computational results are put in relation with the GMR effect, with the aim of enable deductions about the effects that enhance the GMR, at least from a qualitatively point of view. The quantitative predictions will be showed

§ For the sake of notation, a brief comment on Table 1 and Table 2 is required: Cr(1) stands for the monolayer of Cr that is closest to a Fe monolayer; Cr(2) is the central monolayer of the Cr slab, that is, the second of the three Cr monolayers; Fe(1) stands for the external monolayer of the Fe Film; and Fe(2), Fe(3), ..., are the corresponding monolayers inside the Fe slab.

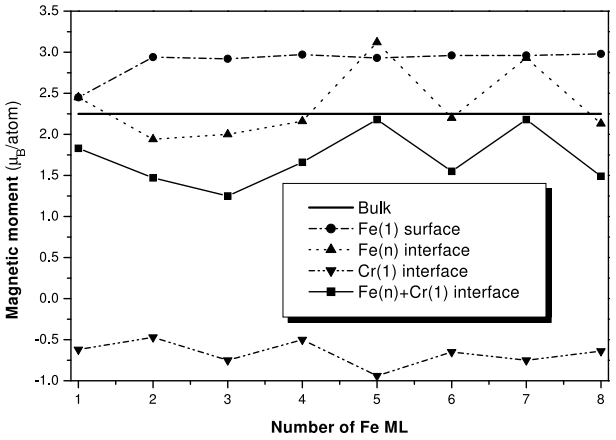

Figure 4. Behavior of the surface (circles) and interface (triangles) Fe magnetic moment versus Fe film thickness. Inverted triangles represent the value of the Cr interface magnetic moment and the squares correspond to the numerical sum of the Fe and Cr interface magnetic moments. Solid line is the magnetic moment of the Fe bulk which is equal to 2.25 μ_B.

in Sec. 3.2. For $n = 5, 7$ we have a special behavior on the Fe/Cr interface (see Table 2), which deserves a more detailed comment. The first characteristic that we obtain, different from what happens for $n = 1, 2, 3, 4, 6, 8$, is that we observe that the majority spins are the main contribution at the Fermi level (see Fig. 5(a)). Notice that the DOS(ε_F) minority spin for $n = 1, 2, 3, 4, 6, 8$ has the corresponding values 3.76, 0.64, 0.44, 0.53, 0.47, and 0.71, while for $n = 5, 7$ they are 0.21 and 0.14, respectively. As can be inferred, these values are much lower than the previous ones (in Fig. 5(b), we can see clearly the criterion employed to consider the magnetic channels to be insignificant for $n = 5, 7$, where the dash dot line is the border line between negligible and appreciable channels). In fact, the lowest value for n=1,2,3,4,6 and 8 is 0.44, which is above the dash dot line. Thus, we observe that the minority spin channels are very small for these two special cases in comparison with the ones seen above. The above comments lead us to conclude that our electronic structure calculations within DOS column graphs presented in Fig. 5 show that there is essentially only one magnetic channel (semimetallic) on the iron-chromium interface for $n = 5, 7$ (see Fig.5(a)-(b) and Table 2) and a very high increase of the magnetism on its interfaces, since the other channel is the one of the minority spin density, quasiequal to zero. Nevertheless, for $n = 1, 2, 3, 4, 6$, and 8 we obtain both kinds of magnetic polarizations: up and down (see Table 1). This situation is very interesting for the GMR effect if we accept that this phenomenon is mainly due to the scattering of the electrons on these interfaces (a feature which will be discussed in Sec. 3.2), that is, the spin-polarized electrons on the one hand, enhance their velocity when they find the magnetic polarizability of the impurity parallel to the magnetic layer, but on the other hand, the spin-polarized electrons diminish their velocity when they find the polarizability in opposite direction. Therefore, we have a spin valve effect in which there is a selection of one of the two possible magnetic channels, and this drives

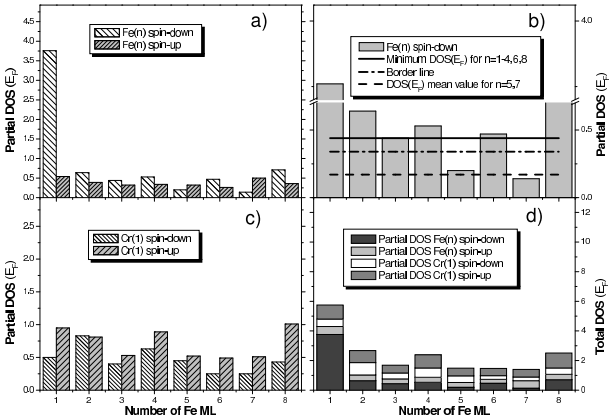

Figure 5. Column graph exhibiting the partial DOS(ε_F) versus the Fe layer thickness for (a) the Fe interface ML spin-up and down, (b) Fe interface ML spin-down and (c) Cr interface ML spin-up and down polarization. (d) show the total DOS(ε_F) as function of the FLT. The dash dot line in (b) establishes a reasonable criterion for considering the minority spin channels insignificant for the case $n = 5, 7$.

a decrease or an increase of the conductivity, depending on whether the electrons are parallel or antiparallel to the magnetic polarization of the interface.

3.2. GMR predictions

So far, the models based on the Boltzmann equation specially developed for describing the multilayer transport properties introduce the potentials as a parameter or consider them in a semiempirical way [8, 9]. The value of this potential is usually taken as a constant however for ultrathin films the potential depends on the thickness of the sample as it was reported in Ref. [30] and consequently, the electronic transport is influenced by the thickness of the sample (not only the thickness of the spacer but also the thickness of the ferromagnetic layer). Contrary to the usual procedure described in literature, in this article, the values of the potentials as a function of the FLT were determined using the DFT methods described earlier (see Fig. 2, Table 1 and Table 2). The dependence of the MR ratio versus the thickness of the ferromagnetic layer d_{Fe} is shown in Fig. 6. The values of the MR ratio obtained for the thickness dependent potential are indicated by full rectangles and they were calculated for a dilute concentration of scattering centers, that is, for c=8.34×10^{-5} [28]. The calculated MR exhibits an oscillatory behavior for a thickness in the range of the x axis displayed by Fig. 6, although the oscillations appear at wrong periodicity compared with the experiments reported in Ref. [3]. In the light of the present calculations, we can conclude that the oscillatory character of the GMR comes mainly from a variable potential distribution through out the thin film, since that the oscillatory behavior of the GMR is hidden as long as the potential is allowed to be constant, like for example in the case of the semiclassical model in which every layer is represented by a quantum well with a constant potential [8]. The MR ratio shown in Fig. 6 exhibits two maxima: the first one at around 4 Å and the second one close to

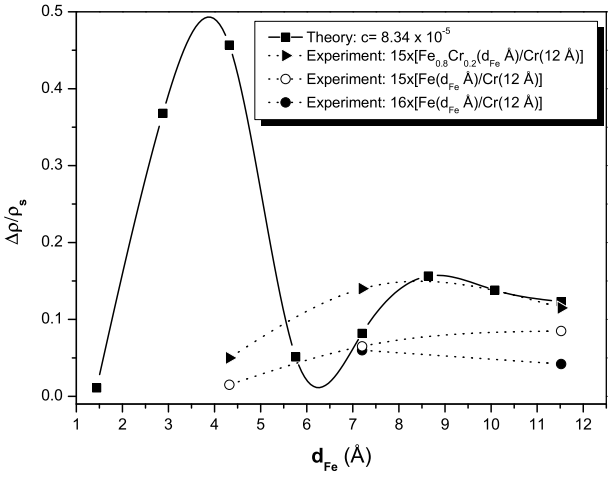

Figure 6. Plot of the calculated (solid line) and experimental [3] (dashed lines) MR ratio as a function of the ferromagnetic layer thickness.

the 8 Å. Thus, although the period of oscillations is wrong compared to the experiment [3], the second maximum agrees quite well with the measurements and we can observe in Fig. 6 that the theoretical and experimental values remain in good agreement in the interval of $d_{Fe} \geq 8$ Å. Only the proper treatment and choice of the potential allows us to obtain the oscillatory behavior even in the semiclassical approach [31]. The important problem, which is up till now omitted in the literature, is the determination of the potential at the interface or even proper treatment of the interface. It is a well known fact that at the interface there exists a significant change of the potential but this change is not of the abrupt character. At the interface there is a transition region where the interdiffusion and the spin mixing take place while the change of the potential should be continuous according to the background.

We note that even though on one hand the GMR effect depends strongly on the temperature [32] and on another hand we are comparing our data (0 K) with the ones reported by Okuno *et al.* (77 K) at different temperatures, the influence of the temperature in the interval [0,77] can be considered negligible [32]. The discrepancy of our results with the experimental ones is less than about 10-15 % for $n \geq 4$, which represents an improvement with respect to other *ab-initio* calculations [33]. The aforementioned small discrepancy can be due to the high number of layers (multilayers) considered in the experiment in comparison with the reduced number of layers (trilayer) of our Fe/Cr sample. For the sake of comparison with the results reported by Okuno *et al.*, it is noteworthy that a remarkable message from our results is the low-dependence behavior of GMR with the number of Fe/Cr layers because the average value of the GMR ratio in function of the Fe layer thickness is around 0.1 for $n \geq 4$ in our calculations and in the experimental results. In order to explain this low-dependence behavior, our proposal consists in considering a quasi-linear dependence of resistance of different number of Fe/Cr layers. Thus, after calculating the GMR ratio, the proportional constant is divided by itself having no appreciable effect in GMR. This tendency

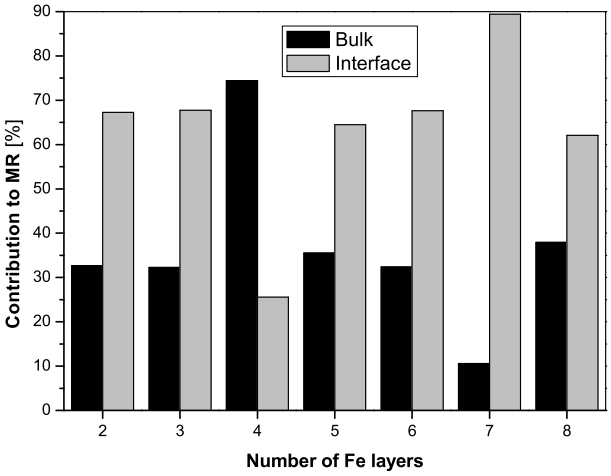

Figure 7. Bulk and interface contribution to the total MR ratio versus the thickness of the ferromagnetic layer for c=8.34×10^{-5}.

disappears for the case of two or three iron monolayers leading to a considerable GMR ratio as shown in Fig. 6, since that the electron states are more localized and thus, they favor an increase of the layer potentials.

We should remind the reader that studies of transport in metallic superlattices (and particularly for trilayers) are affected by many inherent complexities of the material. Many possible complications arise in these types of artificial material, among them, interfacial interdiffusion at various lateral length scales, [34, 35, 36] bulk defects, structural changes as a function of an individual layer and overall thicknesses, different length scales affecting the structure, the boundary conditions on the outermost layers and differences in the magnetotransport along the different directions in the superlattices. But the key point in the mechanism of GMR is the relative importance of bulk and interfacial scattering. Measurements as a function of layer thickness have claimed that the GMR originates from the bulk and that the interfacial roughness does not play a crucial role [37, 38] even in the current perpendicular to plane configuration. Other measurements, in which the interface was modified by the addition of small amounts of interfacial impurities, claim that the interfacial scattering plays a dominant role [39]. The bulk and interface contribution to the total MR ratio as a function of the Fe monolayers is showed in Fig. 7. The results, except for the case n=4, clearly show that the monolayers that belong to the interface dominate the GMR because the potential abruptly changes in this region and it becomes in an important source of scattering. However, in the case n=4 since the potential barrier is less important than the other cases (see in Fig. 2 the square and the inverted-triangle for n=4), the influence of the bulk monolayers become more important. Likewise, in this anomalous case, the reduced contribution of the interface scattering favors a diminishment of the total MR, that is reflected in Fig. 6.

The last measurements reported in Ref. [40] and extensive comparative studies of the growth, structure, magnetization and magnetotransport in Fe/Cr superlattices show

that the intrinsic GMR originates from interfacial scattering and is determined by the interface width [31]. This experimental fact confirms the results shown in Fig. 7 and our earlier conclusion that the interface should be treated physically not as an ideal plane but as a transition zone between different materials where we can observe a mixture of two compounds (interdiffusion) and where not only a significant change of the potential but also a different kind of magnetism take place [6]. The DFT results [41] discussed in Sec. 3.1 confirm the important role of interface, specially the significant increase of magnetic moment at interface for $n = 5, 7$ (see Fig. 4). This fact finds its reflection in a significant change of the potential at interface for different spin polarizations (Fig. 2 and Fig. 5). The difference in interface potential constitutes the main physical reason of different scattering of electrons with different spin orientation and it is the main mechanism responsible for GMR in multilayers.

4. Conclusion

We have shown that using the two combined methods: the *ab initio* methodology for the accurate calculation of the potentials and the semiclassical approach based on the Fuchs-Sondheimer formalism, we obtain the GMR values for the trilayer Fe/Cr/Fe system which oscillates versus the thickness of the ferromagnetic layers. In literature, the GMR oscillations versus the nonmagnetic spacer are emphasized while the role of ferromagnetic layer is considered sporadically. In ordinary semiclassical approach the oscillations of this kind do not exist, however our calculations can predict this oscillatory behavior for ultrathin layers. Our results based on DFT calculations for Fe/Cr system emphasize the very important role of the FLT via thickness dependent potential as well as the contribution of the interface to the GMR ratio. It is worthwhile to notice that the present approach does not contain any semiempirical parameter apart from the calibration constant c.

Acknowledgments

The authors thank the supercomputer center CESGA for access to supercomputers. One of us (M. P.) acknowledges partial support by the Xunta de Galicia, under the project No. PGIDIT02TMT20601PR.

References

[1] M. N. Baibich, J. M. Broto, A. Fert, F. Nguyen Van Dau, F. Petroff, P. Etienne, G. Creuzet, A. Friederich, and J. Chazelas, Phys. Rev. Lett. **61**, 2472 (1988).
[2] P. J. H. Bloemen, M. T. Johnson, M. T. H. van de Vorst, R. Coehoorn, J. J. de Vries, R. Jungblut, J. aan de Stegge, A. Reinders, and W. J. M. de Jonge, Phys. Rev. Lett. **72**, 764 (1994).
[3] S. N. Okuno and K. Inomata, Phys. Rev. Lett. **72**, 1553 (1994).
[4] D. M. Edwards, J. Mathon, R. B. Muniz, and M. S. Phan, Phys. Rev. Lett. **67**, 493 (1991).
[5] P. Bruno and C. Chappert, Phys. Rev. Lett. **67**, 1602 (1991a); **67**, 2592 (1991a).

[6] G. Wiatrowski, D. Baldomir, K. Warda, M. Pereiro, L. Wojtczak, and J. E. Arias, J. Magn. Magn. Mater. **277**, 285 (2004).
[7] P. Zahn, J. Binder, I. Mertig, R. Zeller, and P. H. Dederichs, Phys. Rev. Lett. **80**, 4309 (1998).
[8] R. Q. Hood and L. M. Falicov, Phys. Rev. B **46**, 8287 (1992a).
[9] R. Q. Hood, L. M. Falicov, and D. R. Penn, Phys. Rev. B **49**, 368 (1994a).
[10] P. Zahn, N. Papanikolaou, F. Erler, and I. Mertig, Phys. Rev. B **65**, 134432 (2002).
[11] S. H. Vosko, L. Wilk, and M. Nusair, Can. J. Phys. **58**, 1200 (1980).
[12] H. C. Herper, L. Szunyogh, P. Entel, and P. Weinberger, Phys. Rev. B **68**, 134421 (2003).
[13] W. Kohn and L. J. Sham, Phys. Rev. **140**, A1133 (1965).
[14] V. T. Cherepin, A. A. Ostroukhov, and V. N. Tomilenko, Poverkhnost' (Surface) **6**, 43 (1986).
[15] M. Weinert, J. Math. Phys. **22**, 2433 (1981).
[16] X. Qian and W. Hubner, Phys. Rev. B **67**, 184414 (2003).
[17] J. E. Ortega, F. J. Himpsel, G. J. Mankey, and R. F. Willis, Phys. Rev. B **47**, 1540 (1993).
[18] S. Mirbt, B. Johansson, and H. L. Skriver, Phys. Rev. B **53**, R13310 (1996).
[19] J. L. Pérez-Díaz and M. C. Muñoz, Phys. Rev. B **53**, 13583 (1996).
[20] P. B. Visscher and H. Zhang, Phys. Rev. B. **48**, 6672 (1993).
[21] P. D. Johnson, K. Garrison, Q. Dong, N. V. Smith, D. Li, J. Mattson, J. Pearson and S. D. Bader, Phys. Rev. B. **50**, R8954 (1994).
[22] R. E. Camley and J. Barnas, Phys. Rev. Lett. **63**, 664 (1988).
[23] J. Barnas, A. Fuss, R. E. Camley, P. Grünberg, and W. Zinn, Phys. Rev. B **42**, 8110 (1990).
[24] K. Warda, L. Wojtczak, D. Baldomir, and M. Pereiro, Surf. Rev. Lett. **8**, 271 (2001).
[25] M. Ziese and M. J. Thornton, *Spin Electronics* (Springer-Verlag, Berlin, 2001).
[26] K. Fuchs, Proc. Cambridge Philos. Soc. **34**, 100 (1938).
[27] E. H. Sondheimer, Adv. Phys. **1**, 1 (1952).
[28] J. Kubler, *Theory of Itinerant Electron Magnetism* (Clarendon Press, Oxford, 2000).
[29] S. V. Man'kovsky, D. Baldomir, and M. Pereiro, Int. J. Quantum Chem. **91**, 234 (2003).
[30] K. Warda, L. Wojtczak, G. Wiatrowski, D. Baldomir, M. Pereiro, and J. E. Arias, Czech. J. Phys. **52**, A157 (2002).
[31] M. Pereiro, J. Botana, D. Baldomir, K. Warda, L. Wojtczak, S. Man'kovsky, M. Iglesias, V. Pardo, and J. E. Arias, J. Magn. Magn. Mater. **290-291**, 392 (2005).
[32] M. A. M. Gijs, S. K. J. Lenczowski, and J. B. Giesbers, Phys. Rev. Lett. **70**, 3343 (1993).
[33] K. M. Schep, P. J. Kelly, and G. E. W. Bauer, Phys. Rev. B **57**, 8907 (1998).
[34] E. E. Fullerton, D. M. Kelly, J. Guimpel, and I. K. Schuller, J. Magn. Magn. Mater. **184**, 275 (1998).
[35] J. M. Colino, I. K. Schuller, V. Korenivski, and K. V. Rao, Phys. Rev. B **54**, 13030 (1996).
[36] M. Velez and I. K. Schuller, J. Magn. Magn. Mater. **184**, 275 (1998).
[37] J. E. Mattson, M. E. Brubaker, C. H. Sowers, M. Conover, Z. Qiu, and S. D. Bader, Phys. Rev. B **44**, 9378 (1991).
[38] Z. Q. Qiu, J. E. Mattson, C. H. Sowers, U. Welp, S. D. Bader, H. Tang, and J. C. Walker, Phys. Rev. B **45**, 2252 (1992).
[39] S. S. P. Parkin, Phys. Rev. Lett. **71**, 1641 (1993).
[40] J. Santamaria, M.-E. Gomez, M.-C. Cyrille, C. Leighton, K. K. Krishnan, and I. K. Schuller, Phys. Rev. B **65**, 012412 (2001).
[41] M. Pereiro, D. Baldomir, S. Mankovsky, and J. Arias, Int. J. Quantum Chem. **91**, 245 (2003).

Table 1. Computational results for Fe_n/Cr_3 trilayers (n=1-4,6,8) along with the layer potentials calculated according to Eq. (2) and the relaxation times provided by Eq. (6) with c=8.34×10^{-5}. The symbol m denotes magnetic moment per atom, $\rho_\nu(\varepsilon_F)$ is the density of states at the Fermi level, and $V_{\nu\sigma}$ represents the potential of the majority and minority spin per monolayer.

Trilayer	E_F (eV)	ML	m $\left(\frac{\mu_B}{\text{at.}}\right)$	$\rho_\nu(\varepsilon_F)$ (eV^{-1})		$V_{\nu\sigma}$ (eV)		$\tau^*_{\nu\sigma}$ (10^{-13}s)	
				↑	↓	↑	↓	↑	↓
		Fe(1)	2.45	0.54	3.76	-6.90	-4.90	3.07	0.87
Fe_1/Cr_3	-4.32	Cr(1)	-0.62	0.95	0.50	-7.30	-7.30	2.35	1.58
		Cr(2)	0.62	0.63	0.94	-7.30	-7.30	1.56	2.96
		Fe(1)	2.94	0.13	2.88	-8.19	-5.83	9.05	0.81
		Fe(2)	1.94	0.39	0.64	-7.86	-6.14	3.28	3.27
Fe_2/Cr_3	-3.97	Cr(1)	-0.47	0.81	0.83	-7.69	-7.69	1.65	1.61
		Cr(2)	0.35	0.33	0.50	-7.69	-7.69	4.04	2.67
		Fe(1)	2.92	0.14	2.12	-8.7	-6.3	7.45	0.94
		Fe(2)	2.43	0.15	0.62	-8.5	-6.4	7.28	3.11
Fe_3/Cr_3	-4.32	Fe(3)	2.00	0.32	0.44	-8.3	-6.7	3.58	4.00
		Cr(1)	-0.75	0.53	0.40	-6.3	-6.3	3.75	4.97
		Cr(2)	0.71	0.21	0.23	-6.3	-6.3	4.47	8.65
		Fe(1)	2.97	0.17	2.32	-9.3	-7.3	5.37	0.45
		Fe(2)	2.27	0.28	0.34	-9.3	-7.3	3.26	4.36
		Fe(3)	2.49	0.26	0.57	-9.3	-7.3	3.51	2.60
Fe_4/Cr_3	-4.32	Fe(4)	2.16	0.34	0.53	-9.3	-7.3	2.68	2.79
		Cr(1)	-0.50	0.89	0.63	-7.2	-7.2	1.71	2.42
		Cr(2)	0.50	0.25	0.40	-7.2	-7.2	6.09	3.81
		Fe(1)	2.96	0.08	1.72	-9.4	-7.3	11.16	0.86
		Fe(2)	2.25	0.23	0.36	-9.4	-7.3	3.88	4.11
		Fe(3)	2.41	0.38	0.28	-9.4	-7.3	2.35	5.29
		Fe(4)	2.25	0.41	0.34	-9.4	-7.3	2.18	4.36
Fe_6/Cr_3	-3.95	Fe(5)	2.34	0.28	0.21	-9.4	-7.3	3.19	7.05
		Fe(6)	2.20	0.26	0.47	-9.4	-7.3	3.44	3.15
		Cr(1)	-0.65	0.49	0.25	-7.6	-7.6	2.79	5.47
		Cr(2)	0.58	0.52	0.48	-7.6	-7.6	2.63	2.85
		Fe(1)	2.98	0.04	1.91	-9.3	-7.3	22.81	0.78
		Fe(2)	2.19	0.14	0.36	-9.3	-7.3	6.52	4.11
		Fe(3)	2.35	0.10	0.44	-9.3	-7.3	9.13	3.37
		Fe(4)	2.19	0.14	0.34	-9.3	-7.3	6.52	4.36
		Fe(5)	2.26	0.13	0.30	-9.3	-7.3	7.02	4.94
Fe_8/Cr_3	-3.97	Fe(6)	2.25	0.17	0.39	-9.3	-7.3	5.37	3.80
		Fe(7)	2.35	0.17	0.32	-9.3	-7.3	5.37	4.63
		Fe(8)	2.13	0.36	0.71	-9.3	-7.3	2.54	2.09
		Cr(1)	-0.64	1.01	0.43	-7.7	-7.7	1.32	3.10
		Cr(2)	0.49	0.29	0.46	-7.7	-7.7	4.59	2.89

Table 2. Computational results for Fe_n/Cr_3 trilayers (n=5, 7) along with the layer potentials calculated according to Eq. (2) and the relaxation times provided by Eq. (6) with c=8.34×10^{-5}. The symbols represent the same than in Table 1.

Trilayer	E_F (eV)	ML	m $\left(\frac{\mu_B}{\text{at.}}\right)$	$\rho_\nu(\varepsilon_F)$ (eV^{-1})		$V_{\nu\sigma}$ (eV)		$\tau^*_{\nu\sigma}$ (10^{-13}s)	
				↑	↓	↑	↓	↑	↓
		Fe(1)	2.93	0.17	2.50	-9.4	-7.3	5.04	0.61
		Fe(2)	2.35	0.27	0.92	-9.4	-7.3	3.31	1.61
		Fe(3)	2.41	0.39	0.29	-9.4	-7.3	2.29	5.11
Fe_5/Cr_3	-4.56	Fe(4)	1.79	0.48	0.79	-9.4	-7.3	1.86	1.88
		Fe(5)	3.12	0.32	0.21	-9.4	-7.3	2.79	7.05
		Cr(1)	-0.94	0.52	0.45	-7.4	-7.4	2.77	3.20
		Cr(2)	0.64	0.20	0.14	-7.4	-7.4	7.21	10.30
		Fe(1)	2.96	0.17	2.70	-9.3	-7.3	5.37	0.55
		Fe(2)	2.24	0.46	0.44	-9.3	-7.3	1.98	3.37
		Fe(3)	2.29	0.47	0.22	-9.3	-7.3	1.94	6.73
		Fe(4)	2.21	0.52	0.37	-9.3	-7.3	1.76	4.00
Fe_7/Cr_3	-4.02	Fe(5)	2.27	0.62	0.13	-9.3	-7.3	1.47	11.39
		Fe(6)	1.77	0.55	0.32	-9.3	-7.3	1.66	4.63
		Fe(7)	2.93	0.50	0.14	-9.3	-7.3	1.83	10.58
		Cr(1)	-0.75	0.51	0.25	-7.7	-7.7	2.61	5.32
		Cr(2)	0.50	0.49	0.46	-7.7	-7.7	2.72	2.89

Table 3. The spin-dependent effective mass parameters in units of the free electron mass (m_e).

Trilayer	$m^*_\uparrow$ (m_e)	$m^*_\downarrow$ (m_e)
Fe_1/Cr_3	3.15	3.98
Fe_2/Cr_3	3.55	4.59
Fe_3/Cr_3	3.56	4.62
Fe_4/Cr_3	3.85	5.08
Fe_5/Cr_3	3.92	5.13
Fe_6/Cr_3	3.95	5.17
Fe_7/Cr_3	3.93	5.20
Fe_8/Cr_3	3.93	5.20